Journal of Hydrology 596 (2021) 126030

Contents lists available at ScienceDirect

Journal of Hydrology

journal homepage: www.elsevier.com/locate/jhydrol

Research papers

Stochastic reliability-based risk evaluation and mapping for watershed systems and sustainability (STREAMS)

Allen Teklitz [a], Christopher Nietch [b], Timothy Whiteaker [c], M. Sadegh Riasi [a], David R. Maidment [c], Lilit Yeghiazarian [a,*]

[a] Department of Chemical and Environmental Engineering, University of Cincinnati, OH, USA
[b] USEPA, 26 West Martin Luther King Drive, Cincinnati, OH, USA
[c] The University of Texas at Austin, Center for Research in Water Resources, Austin, TX 78712, USA

ARTICLE INFO

This manuscript was handled by Geoff Syme, Editor-in-Chief, with the assistance of Ashok Mishra, Associate Editor

Keywords:
Risk assessment
GIS
Watershed management
Probabilistic modeling
Watershed modeling

ABSTRACT

Mitigating water contamination, improving water security, and increasing sustainability involve environmental awareness and conscientious decision-making by denizens and stakeholders. Achieving such awareness requires visually compelling geospatial decision-making tools that take into account the probabilistic and spatially distributed nature of water contamination. Inspired by the success of weather maps, this paper presents a novel STochastic Reliability-based Risk Evaluation And Mapping for watershed Systems and Sustainability (STREAMS) tool that produces and effectively communicates the risk of water contamination as maps. STREAMS is integrated with ArcGIS geoprocessing tools and uses physics-based reliability theory to compute the spatial distribution of risk, which is defined as the probability of exceeding a safety threshold of water contamination within a watershed. A quantitative analysis of the efficacy of mitigation strategies is conducted by estimating risk reduction from best management practices throughout the entire watershed. Two case studies at different spatial scales are presented, demonstrating STREAMS application to watersheds with varied properties.

1. Introduction

Humans have been contributing to the deterioration of surface water quality for many decades – one decision, one action at a time. As the world population is projected to grow to 9 billion by 2050 (Gerland et al., 2014; Raftery et al., 2014), the collective negative impact of our decisions is expected to further degrade environmental quality (Goudie, 2018). Mitigating water contamination, improving water security, and increasing sustainability require environmental awareness and conscientious decision-making by denizens and stakeholders. A good analogy (and a goal to work towards) is weather awareness and decision-making based on weather forecasts. Indeed, checking online weather maps has become a part of our everyday lives, as we make decisions on what to wear and where to go based on weather forecasts. To achieve the same level of environmental and water quality awareness, we need the same level of adoption of appropriate geospatial decision-making tools. Our goal in this paper is to demonstrate a geospatial, physics- and probability-based decision-making tool that can be used by water resources professionals for watershed management, and by the general public for recreational decisions. With foundations in reliability theory, this is the first spatially distributed application of the load/capacity reliability-based approach to water quality management.

Weather maps and forecasts have familiarized society with the concept of risk: the question "What is the chance of rain?" has become a common household phrase. Risk is a measure that reflects the inherently stochastic nature of environmental drivers (VanSickle et al., 2009). Like the weather, surface water quality is stochastic because it is driven by random natural factors such as weather and discharge, as well as anthropogenic activities that result in spatially distributed, non-point sources of contamination (Ahn and Merwade, 2014; Dey and Mishra, 2017; Shanhu et al., 2011; Yongfang et al., 2011). For example, non-point sources like agriculture contribute nutrients and fecal microorganisms into the stream networks and are particularly difficult to quantify due to their diffuse nature (Daniel et al., 2011; Yeghiazarian, 2006). Hence, methodologies addressing the probabilistic and spatially distributed nature of surface water quality and security are much needed (Ahmadisharaf and Benham, 2020; Ahmadisharaf et al., 2019; Camacho et al., 2018; Dilks and Feedman, 2004; Langseth and Brown, 2010). This

* Corresponding author.
E-mail address: yeghialt@ucmail.uc.edu (L. Yeghiazarian).

https://doi.org/10.1016/j.jhydrol.2021.126030
Received 25 November 2020; Received in revised form 25 November 2020; Accepted 14 January 2021
Available online 2 February 2021
0022-1694/© 2021 Published by Elsevier B.V.

paper focusing on nutrients (nitrogen), and its companion focusing on microbes and sustainability in the context of water quality (Teklitz et al., 2020) present the first spatially distributed applications of the probabilistic, reliability-based approach to water quality management that addresses these needs. This framework, abbreviated as STREAMS (STochastic Reliability-based Risk Evaluation and Mapping for watershed Systems and Sustainability), facilitates information accessibility and spatial decision-making.

Nitrogen is a primary pollutant of aquatic environments and a focus of multiple efforts for mitigation by the U.S. Environmental Protection Agency, with many states developing nutrient criteria (Chambers et al., 2012; EPA, 1999; Evans-White et al., 2013; Huo et al., 2018; Miltner, 2010; Suplee et al., 2007). Nitrogen contamination is spatially distributed, but standard methods to analyze the risk of contamination and mitigation of impaired waters such as the total maximum daily load (TMDL) process, have been focused on implementation at single points of interest (Borsuk et al., 2002; Camacho et al., 2018; Chin, 2009; Dilks and Feedman, 2004; Franceschini and Tsai, 2008; Langseth and Brown, 2010; Riasi et al., 2018). Expanding risk analysis beyond individual interest points to entire watersheds requires the integration of risk computations into watershed-scale contaminant transport models. The Soil & Water Assessment Tool (SWAT) (Zhang and Zhang, 2011) and Hydrologic Simulation Program – Fortran (HSPF) (Brosch, 2010) are examples of watershed-scale contaminant transport models and can be used to estimate the potential effect of best management practices (BMPs) (Cools et al., 2011; Francesconi et al., 2016; Nelson et al., 2009). Both SWAT and HSPF are physics-based and can inform our understanding of mechanisms and causes of contamination. However, they take a long time to set up and calibrate and do not explicitly consider risk (Bicknell et al., 1997; Neitsch et al., 2011). Data-driven models, on the other hand, while less time-consuming and amenable to probabilistic analysis (Hoque et al., 2012), do not enable mechanistic understanding. Therefore, physics-based, watershed-scale geospatial tools that incorporate probabilistic risk assessments and enable rapid analysis and testing of management scenarios are much needed.

The probability- and physics-based reliability theory that is at the core of STREAMS meets this need. This approach is straightforward to implement and is better suited for decision making than rule-based, deterministic, or arbitrary treatments of uncertainty (Ahmadisharaf and Benham, 2020; Camacho et al., 2018; Langseth and Brown, 2010; Yeonjeong et al., 2007). Reliability theory has been used for risk assessment of various engineered and natural systems, for example see (Abrishamchi et al., 2005; Franceschini and Tsai, 2008; Hamed and El-Beshry, 2004; Maier et al., 2001; Ng and Eheart, 2005; Park et al., 2008; Riasi et al., 2018; Sitar et al., 1987; Thorndahl et al., 2008; Wagner and Gorelick, 1987). In reliability theory, risk is defined as the probability of an unsatisfactory performance under a stressing load, or the probability that the load exceeds the capacity of the system. This probability is also called the probability of failure, with failure defined as any event where the load exceeds the capacity (Haldar and Mahadevan, 2000). In reference to water quality, failure can be, and often is, defined as the event of water contamination exceeding a safety threshold, which could be mandated by regulatory agencies. Despite the geospatial nature of water quality, reliability theory has been applied in water resources management to evaluate risk at single points of interest (Dilks and Feedman, 2004; Franceschini and Tsai, 2008; Riasi et al., 2018; Tung and Mays, 1980). STREAMS presents the first spatially distributed application of reliability theory to water quality management.

STREAMS produces the predicted consequence of decisions, thereby allowing scenario analysis. It is designed to answer two types of questions: (1) “what is the probability of exceeding the water quality criterion anywhere in the watershed”, and (2) “how much would this probability change if we implement strategy X, and where will this change be the largest?”. The efficacy of mitigation strategies is also assessed. To build STREAMS, we expand the existing modeling and computational capabilities of ArcGIS, specifically the geoprocessing tool

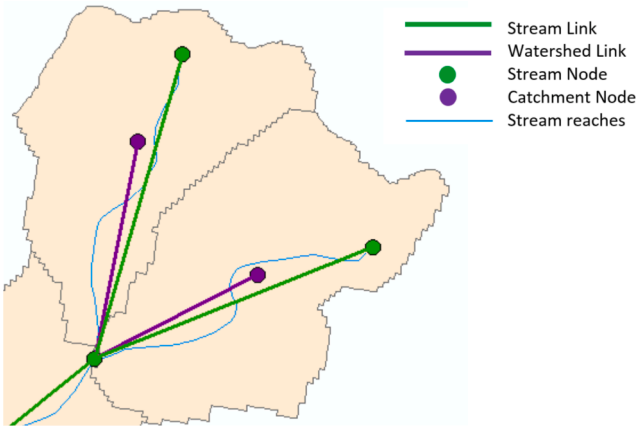

Fig. 1. The Schematic Processor passes loads from the catchments into the streams (modified from Whiteaker (2006)). Green links represent streams and purple the overland runoff. Purple nodes are placed at the centroid of respective sub-catchments. Upstream contributions are summed at green nodes. (For interpretation of the references to colour in this figure legend, the reader is referred to the web version of this article.)

called the Schematic Processor (SP), which has been developed to simulate the physics of contaminant transport in flow networks (Whiteaker (2006)). We use the analytical solutions of transport equations and the first-order approximation method to derive the first and second moments of the capacity and loading. We account for covariance between the load and capacity in the transport equations, and consider uncertainty both in the system capacity and the load on the system, as opposed to incorporating uncertainty in loading only (Yang et al., 2014). This information is then used to compute the probability of water contamination using the First Order Reliability Method. Because GIS serves as a platform to integrate a watershed-scale nitrogen transport model with reliability-based risk assessment, the outcome is an intuitive and visually compelling decision-making tool that can generate easily comprehensible visualizations of water quality and of watershed management strategy efficacy. The resulting map products allow watershed managers to make decisions based on risk assessment at the watershed scale, as well as enable virtual experimentation of the impact of various decisions on water quality.

This paper is structured as follows. Section 2 covers the STREAMS methodology developed in this paper. First, we review the characteristics of the ArcGIS SP and its use in modeling environmental processes (Section 2.1). How the SP is used to model nitrogen sources is described in Section 2.2. The techniques used for streamflow estimation are covered in Section 2.3. Nitrogen fate and transport are described in Section 2.4 followed by model calibration in Section 2.5. Load variability is modeled using the first-order approximation method (Section 2.6). STREAMS uses the computed nitrogen dynamics and the variability in load and capacity to calculate the probability of contaminants exceeding a safety threshold (risk), Section 2.7. The results are visualized as a risk map, which is the STREAMS output. STREAMS is demonstrated in application to two watersheds in southwestern Ohio - the Shepherd Creek watershed (Section 3) and the Upper East Fork Watershed (UEFW) of the Little Miami River (Section 4). The effects of BMP implementation are examined throughout each watershed in their respective sections. STREAMS results and maps illustrate the projected risk reductions and can be used to support watershed management decisions.

2. STREAMS modeling framework

2.1. Schematic Processor (SP) in ArcGIS

The STREAMS modeling framework builds on the ArcGIS SP

developed by Whiteaker (2006). The SP is a suite of geoprocessing tools for ArcGIS that uses a link-and-node schematic representation (schematic network) of hydrologic flows. The schematic network of a watershed is generated by placing a node at the centroid of every catchment, and at the beginning and the end of every reach. Links connect nodes and represent streams, as well as any surface runoff from sub-catchments (Fig. 1). In other words, nodes and links symbolize landscape features such as hillslopes, lakes, streams, and surface runoff paths. The National Hydrologic Dataset (NHDPlus) can be used to generate the schematic network of a given watershed automatically, as it provides the stream network and catchments (NHDPlus High Resolution at https://www.usgs.gov/core-science-systems/ngp/national-hydrography/nhdplus-high-resolution; and http://www.horizon-systems.com/NHDPlus/NHDPlusV2_home.php where the high resolution is not available) (see for example Tavakoly Zadeh (2014) and Johnson et al. (2013)). For areas smaller than a single NHD catchment, streams and sub-catchments can be delineated from the digital elevation model, which produces a local-scale, highly detailed schematic network. We use both approaches in this paper: the UEFW was processed using NHD, while the schematic network of the smaller Shepherd Creek watershed was obtained from the digital elevation model.

Each SP feature (link or node) can perform different processing operations such as receiving, passing, and executing various mathematical calculations. The inputs for each SP feature are processed and the result becomes its output, which is then used as the input for downstream features. Because of this design, different transport models can be implemented within the SP. Our interest in this paper is surface water contamination with inorganic nitrogen; hence a nitrogen transport model is implemented in the SP (see Section 2.3). Point sources of water contamination can be represented by placing a node at the location of the source; then using a link to connect it to respective downstream nodes in the schematic network. Non-point sources are represented by a node placed at the centroid of each catchment and are connected to its outlet node by a link.

2.2. Nitrogen sources

STREAMS accounts for all nitrogen sources and inputs at any node:

$$L_{total} = L_{NPS} + L_{PS} + L_u \tag{1}$$

where L_{total} is the total input load at a given node, L_{NPS} and L_{PS} are the non-point and point-source contributions respectively; and L_u is the computed incoming load from upstream features of the network. All parameters are listed in the appendix.

Annual point-source contributions are calculated from the National Pollutant Discharge Elimination System (NPDES) permits or values from the literature. Non-point source contributions are computed based on export coefficients that represent the loss of contaminant mass per unit area per unit of time (usually a year), categorized by land use. They are typically estimated using regression equations, field monitoring, or mechanistic modeling (Beaulac and Reckhow, 1982; Lin, 2004; Robertson and Saad, 2011; Shrestha et al., 2008; U.S.EPA, 2001). In STREAMS, non-point source contaminant loading is calculated as:

$$L_{NPS} = \sum_{i=1}^{m} \in_i A_i \tag{2}$$

where $\in_i$ is the export coefficient for the respective land use of areaA_i for m different land uses. This paper uses land uses reported in the National Land Cover Database (NLCD) (Alarcon et al., 2010).

2.3. Streamflow estimation in ungauged locations

Flow is estimated for every stream in the network. There are many methods to model streamflow, including models based on the unit hydrograph (Jakeman et al., 1990), rainfall-runoff (Young, 2006), and data-driven approaches (Besaw et al., 2010; Wang et al., 2008) that allow computing streamflow statistics (Koltun and Whitehead, 2002; Martin and Arihood, 2010; Stuckey et al., 2012; Vogel et al., 1999). STREAMS uses the best-fit regression equation for the average flow from Koltun and Whitehead, 2002 that can be readily applied to the entire watershed. As this equation estimates the mean flows, the output for each modeled year is scaled based on the average flow at available monitoring stations. Regression equations are applied in every catchment; upstream loads are added at nodes and passed downstream.

2.4. Nitrogen transport

The 1D nitrogen transport model is based on the concept of spiraling length, which represents the distance a dissolved nutrient molecule travels in the water column before it is removed by a biotic process. The model is directly related to the first order decay model that can be used with many contaminants. The mathematical basis of spiraling length has the following form (Runkel, 2007; Stream Solute Workshop, 1990):

$$C_y\left(\frac{Q_y}{Q_0}\right) = C_0 e^{-\frac{y}{S}} \tag{3}$$

where C_0 and Q_0 are respectively the initial concentration and flow, y is the travel distance, C_y and Q_y are respectively the concentration and flow at distance y, and S is the spiraling length. Flow is assumed uniform within each link of the schematic network (*i.e* $Q_0 = Q_y = Q$). This assumption is imposed by the SP, which calculates the additional flow at the nodes, and not at links. For an area that has mostly full-flowing channels, it is reasonable to assume that dispersion is negligible, that temporary storage areas are negligible, and that uptake occurs only in the main channel (Gandolfi et al., 2001). Nitrification of ammonia from both point and non-point sources is assumed to happen instantly. This leads to the following relation between the spiraling length and uptake rate (Runkel, 2007; Stream Solute Workshop, 1990):

$$S = \frac{V}{\lambda} \tag{4}$$

where V is the flow velocity and λ the first order uptake rate. Throughout the schematic network, each streamflow regime has a specific spiraling length (Ensign and Doyle, 2006; Schwarz et al., 2009); and in this study, nitrate is of concern as the nitrogen species predominant in rivers (Hall et al., 2009; Taylor et al., 2005).

Load is calculated in every reach by multiplying both sides of Eq. (3) by flow and applying the same assumptions as for Eq. (4):

$$L_{\mathbb{r}} = \left[L_0 e^{-\frac{V}{S}t} \right]_{\mathbb{r}} \tag{5}$$

where for every reach $\mathbb{r}$, $L_{\mathbb{r}}$ is the contaminant load at distance y, t is the travel time (*i.e.* the time it takes to travel distance y at velocity V such that $t = V/y$), and L_0 is the initial load. As loads are passed through the schematic network, the value of L_{total} (Eq. (1)) at the upstream node of the subsequent stream link becomes the initial load L_0 (Eq. (5)) for that link. Thus, STREAMS uses Eq. (5) to compute the nitrate fate and transport at every link throughout the network, while incorporating the physical features of individual streams (length y, velocity V, and travel time t). This produces the spatial load distribution throughout the watershed.

2.5. Calibration

The Nash-Sutcliffe Efficiency (NSE) coefficient (Nash and Sutcliffe, 1970) is used to evaluate model performance. The NSE indicates how well the observed data and model results fit a 1:1 line; the closer the NSE

is to 1, the more accurate the model is (Moriasi et al., 2007). The calibration parameters are the export coefficients that modulate the NPS load input throughout the system for both case study watersheds. For the UEFW, the spiraling length at various flows is also used as a calibration parameter. Given the reported ranges for spiraling length and export coefficients, Excel's optimization functionality is used to calibrate the model by maximizing the NSE for the first year of data (the rest of the data are used for validation). The resulting spiraling lengths and export coefficients are then used in modeling load variability and in calculating risk, as described in sections 2.6 and 2.7, respectively.

2.6. Modeling load variability

There are many ways to calculate variability, ranging from computationally intensive methods such as Monte Carlo simulations to approximation methods (Beck, 2013; Mishra et al., 2019; Shirmohammadi, 2006; Tsai and Franceschini, 2005). STREAMS uses first-order approximation to calculate the mean and coefficient of variation (*CV*) of the response variable (the load). For highly non-linear problems, modifications of the first-order approximation can be employed (Kriegesmann, 2012; Maskey and Guinot, 2003).

Generally, in the first-order approximation method,

$$Z = g(X_1, X_2, \cdots, X_n) \tag{6}$$

where Z is a function of random variables $X_1, X_2, \cdots, X_n$. The mean of Z is approximated as:

$$\mu_Z \approx g(\mu_{X_1}, \mu_{X_2}, \cdots, \mu_{X_n}) \tag{7}$$

where μ_{X_i} is the mean of X_i, $i = 1,\ldots,n$. In general, the variance of Z is:

$$Var(Z) \approx \sum_{j=1}^{n}\sum_{k=1}^{n} \frac{\partial g}{\partial X_j}\frac{\partial g}{\partial X_k} Cov(X_j, X_k) \tag{8}$$

where *Cov()* is the covariance. If variables $X_1, X_2, \cdots, X_n$ are independent, Eq. (8) simplifies to:

$$Var(Z) \approx \sum_{j=1}^{n} \left(\frac{\partial g}{\partial X_j}\right)^2 Var(X_j) \tag{9}$$

Note that all derivatives in (8) and (9) are evaluated at the mean values. For each link, the mean contaminant load is obtained by applying Eq. (7) to the transport Eq. (5):

$$\mu_{L_{\mathbb{r}}} = \mu_{L_0} e^{-\frac{\mu_V}{\mu_S}\mu_t} \tag{10}$$

where $\mu_{L_{\mathbb{r}}}$ is the mean load at the end of reach $\mathbb{r}$, μ_{L_0} is the mean initial load for the reach, μ_V is the mean flow velocity, μ_S is the mean spiraling length, and $\mu_t$is the mean travel time. STREAMS applies this at the links. Here, remembering that the total load of the upstream node is used as the initial load for the stream link, μ_{L_0} is obtained by applying Eq. (7) to Eqs. (1) and (2):

$$\mu_{L_0} = \sum_{i=1}^{m} \mu_{\epsilon_i} A_i + \sum_{\imath=1}^{\aleph} \mu_{L_{PS\,\imath}} + \sum_{\iota=1}^{\eta} \mu_{L_{u\,\iota}} \tag{11}$$

where μ_{ϵ_i} is the mean export coefficient in area A_i, $\mu_{L_{PS\,\imath}}$is the $\imath$th mean point-source input of $\aleph$ point-sources, and $\mu_{L_{u\,\iota}}$ is the mean upstream load for the ιth upstream branch, and η is the number of upstream input branches. It then follows that $Var(L_0)$ is calculated from Eqs. (1) and (9).

$$Var(L_0) = Var(L_{NPS}) + Var(L_{PS}) + Var(L_u) \tag{12}$$

STREAMS applies Eqs. (11) and (12) at the nodes. Note that in the SP design, L_{NPS} are symbolized by nodes placed at catchment centroids, which do not receive input from upstream since there are no upstream links, *i.e.* $Cov(L_{NPS}, L_u) = 0$. Further, point source inputs are assumed to be independent from L_{NPS} and L_u, *i.e.* $Cov(L_{NPS}, L_{PS}) = 0$ and $Cov(L_{PS}, L_u) = 0$.

The variance of loads from non-point sources $Var(L_{NPS})$ can be computed at catchment nodes based on Eqs. (2) and (8). It is assumed that areas A_i are independent of one another (*i.e.* $Cov(A_j, A_k) = 0$ for $j|j \in \mathbb{Z} and 1 \le j \le m$, $k|k \in \mathbb{Z} and 1 \le k \le m$ where $\mathbb{Z}$ is the set of all integers), and of export coefficients ϵ_i (*i.e.* $Cov(A_i, \epsilon_i) = 0$ for $i|i \in \mathbb{Z} and 1 \le i \le m$) . Note that the export coefficients are not assumed independent of one another. Then,

$$Var(L_{NPS}) = \sum_{j=1}^{m}\sum_{k=1}^{m} \frac{\partial L_{NPS}}{\partial \epsilon_j}\frac{\partial L_{NPS}}{\partial \epsilon_k} Cov(\epsilon_j, \epsilon_k) \tag{13}$$

To calculate the variance of loads from point sources $Var(L_{PS})$, reported concentrations (C_{PS}) and flows (Q_{PS}) are used where available. Since $L_{PS} = Q_{PS}C_{PS}$, Eq. (9) can estimate $Var(L_{PS})$ as:

$$Var(L_{PS}) = Var(Q_{PS})\mu_{C_{PS}}{}^2 + \mu_{Q_{PS}}{}^2 Var(C_{PS}) \tag{14}$$

where $\mu_{C_{PS}}$ and $\mu_{Q_{PS}}$ are the mean of the measured concentration and flow data respectively and $Var(C_{PS})$ and $Var(Q_{PS})$ is the variance in the measured concentration and flow data respectively.

To calculate the variance of loads from upstream links $Var(L_u)$ at any node, while keeping in mind that $L_u = \sum_{\iota=1}^{\eta} L_{u\iota}$, Eq. (8) is applied:

$$Var(L_u) = \sum_{j=1}^{\eta}\sum_{k=1}^{\eta} \frac{\partial L_u}{\partial L_{uj}}\frac{\partial L_u}{\partial L_{uk}} Cov(L_{uj}, L_{uk}) \tag{15}$$

Note that in Eq. (15), $Cov(L_{uj}, L_{uk}) = Var(L_{uj})$ for $j = k$.

The variance in the load at the end of each stream link $\mathbb{r}$ is obtained from Eqs. (8) and (5):

$$\begin{aligned} Var(L_{\mathbb{r}}) = \frac{e^{-\frac{2\mu_t\mu_V}{\mu_S}}}{\mu_S{}^4}\Big[& -2Cov(L_0, V)\mu_{L_0}\mu_S{}^3\mu_t - 2Cov(L_0, t)\mu_{L_0}\mu_S{}^3\mu_V \\ & +2Cov(L_0, S)\mu_{L_0}\mu_S{}^2\mu_t\mu_V + 2Cov(V, t)\mu_{L_0}{}^2\mu_S{}^2\mu_t\mu_V \\ & -2Cov(V, S)\mu_{L_0}{}^2\mu_S\mu_t{}^2\mu_V - 2Cov(S, t)\mu_{L_0}{}^2\mu_S\mu_t\mu_V{}^2 \\ & +\mu_S^4 Var(L_0) + \mu_{L_0}{}^2\mu_t{}^2\mu_V{}^2 Var(S) + \mu_{L_0}{}^2\mu_S{}^2\mu_t{}^2 Var(V) \\ & +\mu_{L_0}{}^2\mu_S{}^2\mu_V{}^2 Var(t)\Big] \end{aligned} \tag{16}$$

where $Var(L_0)$ is the variance at the stream link's upstream node obtained from Eq. (12). Finally, the coefficient of variation ($CV_{L_{\mathbb{r}}}$) of the load in stream link $\mathbb{r}$ is calculated as:

$$CV_{L_{\mathbb{r}}} = \frac{\sqrt{Var(L_{\mathbb{r}})}}{\mu_{L_{\mathbb{r}}}} \tag{17}$$

Note that the load mean and variance are calculated and passed through every feature in the schematic network. The accuracy of first-order approximation method was verified using Monte Carlo simulations; and results for each case study are reported in sections 3.2 and 4.2. In the next section, we describe the use of $CV_{L_{\mathbb{r}}}$ in risk calculations.

2.7. Calculating risk

As mentioned in the introduction, risk is defined as the probability p_f that contaminants in water exceed a safety threshold. It can be computed for every link in the schematic network as:

$$p_{f_{\mathbb{r}}} = P(R_{\mathbb{r}} < L_{\mathbb{r}}) \tag{18}$$

where $p_{f_{\mathbb{r}}}$ is the probability of failure for link (reach) $\mathbb{r}$, $R_{\mathbb{r}}$ is the capacity or resistance in reach $\mathbb{r}$, which describes the load that a stream represented by the respective link can support and remain safe, and $L_{\mathbb{r}}$ is the contaminant load in that stream link. Fig. 2A illustrates this concept for the case when both capacity R and load L are random variables (here, R and L are generalized). The overlap between the two probability

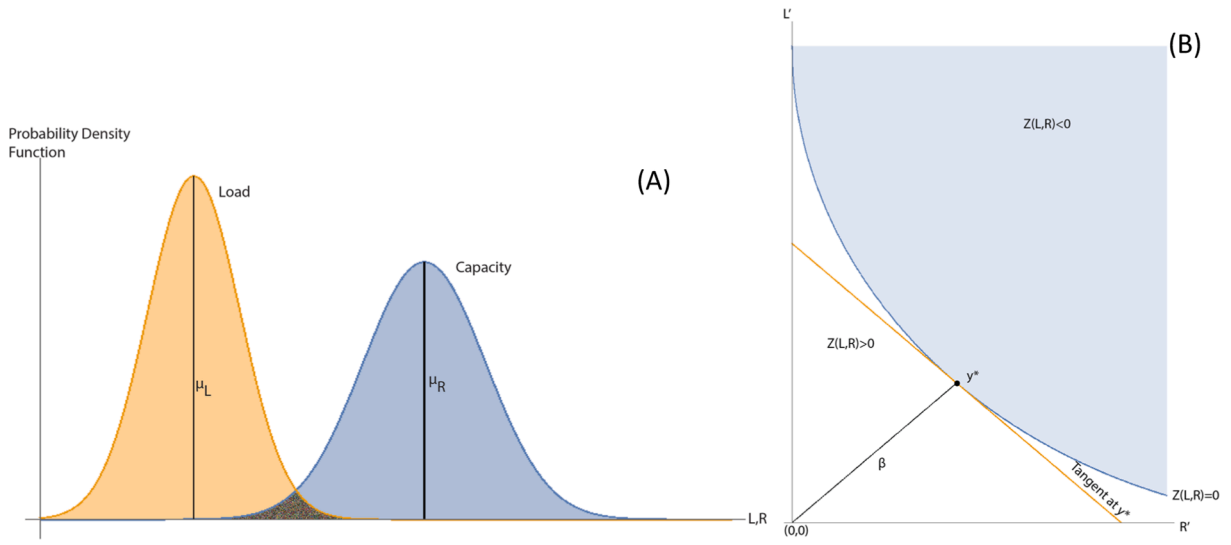

Fig. 2. (A) Load and capacity are both random variables. The shaded area where L > R is the failure region. (B) Concept behind the First Order Reliability Method (FORM) based on Sitar et al. (1987). L and R are transformed into standard normal variates *L'* and *R'*. In the standard normal space, the most probable point of failure (y*) is the point on the graph of the performance function (*Z = R-L)* that is closest to the origin. (β) is the minimum distance between the origin and the performance function. The shaded space is the failure region, and the un-shaded space is the safe region.

distributions is the failure region where $R < L$. Below we describe how p_f is calculated in two cases: when R and L are independent of each other, and when they are dependent. For both cases we first need to determine their moments.

Stream capacity is defined as $R_{\mathbb{r}} = QC_T$, where C_T is the safety concentration threshold that should not be exceeded. This paper usesC_T = 1.1 mg/L for total dissolved inorganic nitrogen (TIN) (Miltner (2010)). TIN is the sum of ammonia, nitrate, and nitrite nitrogen (in flowing natural waters that are downstream of point source mixing zones, nitrate dominates the TIN speciation). Then the mean stream capacity $\mu_{R_{\mathbb{r}}}$ for a given reach $\mathbb{r}$ is:

$$\mu_{R_{\mathbb{r}}} = \mu_{Q_{\mathbb{r}}} C_T \tag{19}$$

where $\mu_{Q_{\mathbb{r}}}$ is the mean flow in reach $\mathbb{r}$. To calculate the coefficient of variation in capacity CV_R, the linear relationship in Eq. (19) can be used to first determine the variance (Haldar and Mahadevan, 2000):

$$Var(R_{\mathbb{r}}) = Var(Q_{\mathbb{r}}) {C_T}^2 \tag{20}$$

which can then be used similarly to Eq. (17) to calculate $CV_{R_{\mathbb{r}}}$.

Nitrogen loads can be approximated by the lognormal distribution (Cowan et al., 2019; Levy et al., 2017; Limpert et al., 2001). Data available from the case studies used in this paper passed the Kolmogorov–Smirnov test for lognormality at 5% significance at every monitoring location. Assuming that R and L are lognormal and independent from each other, p_f can be calculated analytically as (Haldar and Mahadevan, 2000):

$$p_f = 1 - \Phi\left(\frac{ln\left[\left(\frac{\mu_R}{\mu_L} \right) \sqrt{\frac{1+{CV_L}^2}{1+{CV_R}^2}} \right]}{\sqrt{ln\left(1+{CV_R}^2\right) + ln\left(1+{CV_L}^2\right)}} \right) \tag{21}$$

where $\Phi(.)$ is the cumulative distribution function of the standard normal variate.

The independence assumption may be appropriate in some cases, for example in single flow processes within individual streams. Generally, including when the independence assumption does not hold, p_f can be computed using techniques such as the First- or Second-Order Reliability Methods (FORM/SORM) or Monte-Carlo simulations (Sitar et al., 1987).

Here we employ FORM, which uses the Taylor expansion of the so-called performance function $Z = R\text{-}L$ to approximate p_f (Fig. 2B) (Sitar et al., 1987; Bourinet et al., 2009). A detailed description can be found in Haldar and Mahadevan (2000) and Riasi et al. (2018). Briefly, the algorithm transforms the random variables into standard normal variates and minimizes the distance between the performance function and the origin to determine the most likely failure point. Probability of failure is then approximated as:

$$p_f = 1 - \Phi(\beta) \tag{22}$$

where β is the shortest distance between the origin and the graph of the performance function (Fig. 2B). We performed FORM using the Finite Element Reliability Using Matlab (FERUM) software developed by Bourinet et al. (2009). The required inputs for each stream link $\mathbb{r}$ are mean load ($\mu_{L_{\mathbb{r}}}$), mean capacity ($\mu_{R_{\mathbb{r}}}$), *CV* of load ($CV_{L_{\mathbb{r}}}$), *CV* of capacity ($CV_{R_{\mathbb{r}}}$), the correlation matrix and the distribution type (lognormal).

3. Case study 1 – Shepherd Creek

Our first case study is the Shepherd Creek watershed in Southwest Ohio. Using STREAMS, the probability of exceeding the TIN standard is computed and mapped for the entire drainage network. The mapped results are useful for visualizing the spatial distribution of risk and for identifying areas that can be targeted for remediation. BMP implementation is simulated and potential reduction in risk is computed to evaluate BMP efficacy.

3.1. Study area

The Shepherd Creek watershed is located in Cincinnati, Ohio. The watershed spans 1.85 km^2 (457 acres) and is about one-third mature deciduous forest within a city park, two-thirds residential, and has horse pastures. There are six stations that monitor TIN in the watershed; sampled on a monthly basis from 2005 to 2010 by the USEPA (Roy et al., 2006; Roy and Shuster, 2009). The sampling program included more frequent sampling targeting several storm events. The water quality monitoring data can be accessed using http://data.cuahsi.org, by specifying an area, chemical species of interest, and a date range (Ames et al., 2012; Tarboton et al., 2009) (Safwat, 2014; Yeghiazarian et al., 2013). The watershed and monitoring stations are shown in Fig. 3.

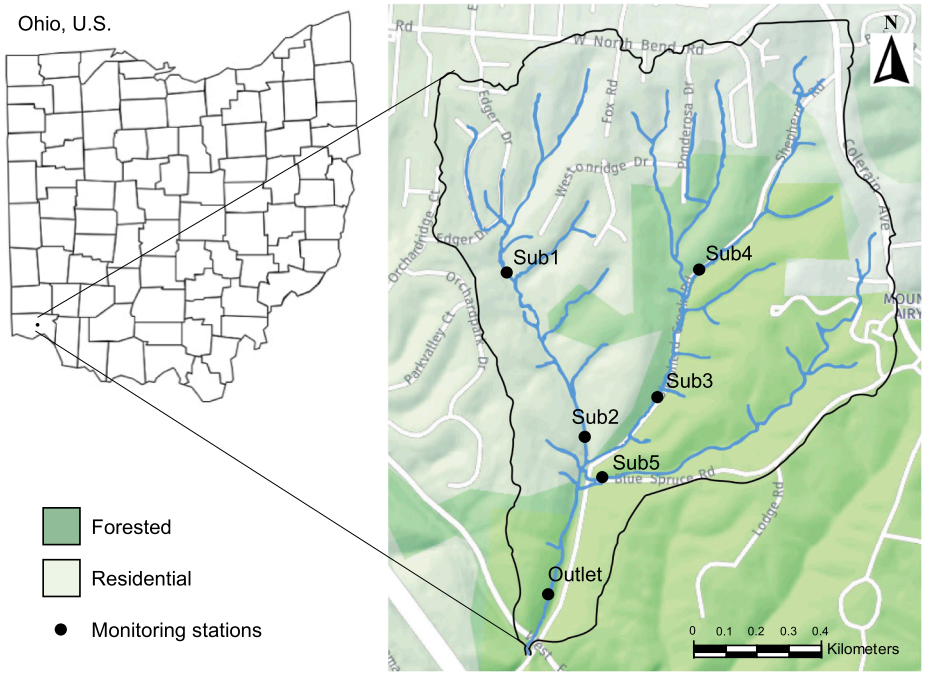

Fig. 3. Shepherd Creek Watershed (Reprinted from Riasi et al. (2018) with permission). There are six monitoring stations within the watershed monitoring the outlet and the various branches.

3.2. Model parameters and calibration

The monitoring stations have 6 years of data. Daily averages were available for flow; nitrogen sampling occurred monthly. Several storms were sampled additionally, which lead to the full flow distribution curve being well represented (Teklitz, 2016). To calculate loads from various land uses, the export coefficients from Table 1 are used in Eq. (10). These values (which fall within the published range of nitrogen export coefficients (Lin, 2004; Saad et al., 2011; Schwarz et al., 2009) were produced by calibrating the model with the 2005 data and using export coefficients as calibration parameters.

The value of spiraling length is the mean estimate taken from Ensign and Doyle (2006), where the spiraling length is 478 m for first-order streams. Velocities from the NHDplus dataset (McKay et al., 2012) were used, which are estimated using the methodology from Jobson (1996). Fig. 4 demonstrates nitrogen fate and transport model performance for years 2005–2010, which are based on the modeled load output compared to the measured load that was estimated from the daily flow data and measurement samples. The natural logarithm of the load was chosen as the model uses lognormal distributions in the estimation of risk. The NSE for all years is satisfactory, as shown in Fig. 4. For the flow, as discussed in section 2.3, the weighting factors for 2005–2010 were derived from NLDAS Station X323-Y113 (located 500 m East of the watershed boundary, using all data starting from 1979) hourly surface runoff data and were equal to 1.1, 1.2, 0.96, 1.6, 0.90, and 1.0 for each respective year. These values are for the annual average and applied to the results from the Koltun and Whitehead, 2002 regression equations. The estimated flows at all 6 stations for all years were also satisfactory with NSE of 0.55.

Table 1
Export coefficients of nitrogen used for various land use types in Shepherd Creek.

Land Use (Based on NLCD2006)	Mean Export Coefficient μ_{ϵ_i} (kg of TIN/ha/year)	
	Reported Range in Literature	Used in this Study
Forested	1 – 15	3.2
Row Crops	2 – 80	14.9
Mixed Agriculture	2 – 41	10.0
Developed, Open	0.1 – 7	4.8
Developed, Low Intensity	1.9–11	4.8
Developed, High Intensity	1.9 – 14	2.1

The estimated coefficients of variation (*CV*) for parameters needed to calculate risk are presented in Table 2a and 2b. To estimate *CV* of flow (Q), the average *CV* of flows at the monitoring stations was used as available. If measurement data are not available, the standard error is often reported and can be used to estimate the CV (*i.e.* the equation this paper uses is from Koltun and Whitehead, 2002 and reports a standard error of 11.4 for 215 observations). For stream velocity V there were no measurement data available in or near the study areas, so the velocity estimate was obtained from the NHDPlus means stream velocity estimate which is based on Jobson (1996) which reports a Root Mean Square Error (RMSE) (which can be related to the variance at the mean) between 0.157 m/s and 0.21 m/s. For the spiraling length, the mean (727 m for NO_3), median (236 m for NO_3), and interquartile range (102–758 m for NO_3) is reported in Ensign and Doyle (2006). From these values, the coefficients of variation based on a lognormal distribution can be estimated (Table 2a). The model uses an annual time step (reflected in Tables 2a and 2b). Similarly, to determine the CV for export coefficients from the various land uses, the reported mean, median, and interquartile range is used where available (see Table 2b). Wherever only the range is available (*e.g.*, developed, low intensity; and developed, high intensity), the minimum and maximum of the range is assumed to be the fifth and ninety-fifth quartile respectively on a lognormal distribution, from which the CV can be estimated.

To compute Eqs. (11), (14), and (15), covariances between various factors are also needed. This paper uses estimates of the correlation between factors to compute covariances (Table 3). The FORM algorithm also needs the correlation between the capacity and load to compute Eq. (18). Covariance is related to correlation (ρ) by $\rho_{X,Y} = \mathrm{Cov}(X,$

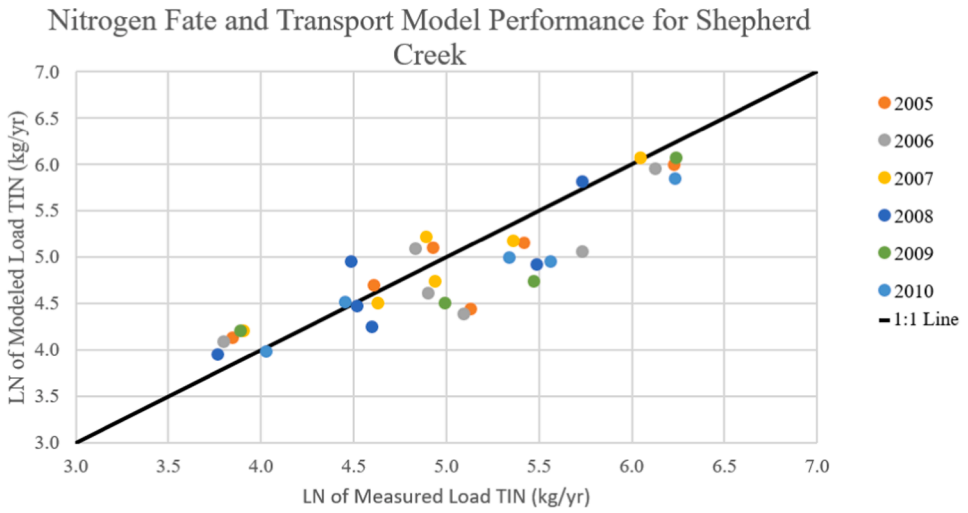

Year	2005	2006	2007	2008	2009	2010
NSE Load	0.82	0.64	0.94	0.71	0.77	0.63
NSE LN(Load)	0.75	0.60	0.88	0.72	0.67	0.79

Fig. 4. Model performance across all years based on the natural logarithm of the measured and modeled DIN loads. Calibration was done with the year 2005 data using the comparison of the natural logarithm of the loads; the same model was implemented using the remaining years for validation. Models for all years have satisfactory performance.

Table 2a
Estimated coefficients of variation for yearly time step.

Parameter	Estimated Coefficient of Variation (*CV*)
Flow(Q)	2
Stream Velocity(V)	0.45
Spiraling Length(S)	2.9

Y)/($Stdev(X)Stdev(Y)$), where $Stdev()$ is the standard deviation. Due to the lack of relevant data to directly calculate several of these values for this watershed, this paper employs several conservative assumptions and estimates. The in-stream velocity is a function of streambed geometry (slope, hydraulic radius) and conditions, so is assumed to have no covariance with initial loading. Travel time in stream is a function of the velocity and stream length so this paper conservatively selects a correlation of 1 for velocity and travel time. The travel time is not related to the initial load or spiraling length, therefore respective covariance values are set to zero. Through Eq. (4), S and V are directly related, so this paper conservatively assumes complete correlation between them. As spiraling length S is related to stream parameters instead of loading factors, L_0 and S are assumed to be independent.

Table 2b
Estimated coefficients of variation for various land uses for yearly time step.

Land Use (Based on NLCD2006)	Mean, Median, Interquartile Range of Export Coefficients (kg/ha/yr) from Reckhow et al. (1980)	Estimated Coefficient of Variation (*CV*)
Forested	2.86, 2.46, 1.19	0.59
Row Crops	16.09, 9.0, 18.05	1.5
Mixed Agriculture	1.13, 0.91, 0.88	0.74
Developed, Open	9.97, 5.5, 7.36	1.5
	Range of Export (kg/ha/yr) from (Loehr, 1989) in (Lin, 2004)	
Developed, Low Intensity	1.9–11	0.57
Developed, High Intensity	1.9–14	0.67

To determine the correlation between incoming upstream loads at any node, the flow and concentration that define load calculations need to be considered. The correlation between upstream flows is often high (a range of 0.5 to nearly 1 is reported in Messinger and Paybins (2014)), however concentrations can have mixed relationships but are often negatively correlated (Arheimer et al., 1996; Arheimer and Liden, 2000). In Shepherd creek, some of the sampling was performed where samples were taken from all stations within a short time frame (however, this sort of data are not available in the UEFW). We use the mean correlation between loads at Sub2, Sub3, and Sub5 to estimate the correlation between upstream loads and for export coefficients, assuming they have the same value. The obtained value of 0.17 (Table 3) falls between the positive flow correlation and negative concentration correlation. This is also the value we use for different land uses in a catchment. The correlation between the capacity R and loading L across Shepherd Creek was computed directly from available data.

To validate the accuracy of the first-order assumptions for variance across the network, we use a Monte Carlo simulation using the same processing network and input parameters. The computed variance from the Monte Carlo simulation is then compared at every link to the output of the first-order model. This produced a NSE of 0.57 across all links for variance.

3.3. Results and discussion

3.3.1. Risk maps

The risk map for Shepherd Creek, produced by STREAMS for years 2005–2010, is presented in Fig. 5. It shows the probability that the TIN in the individual streams is greater than the stream capacity.

The STREAMS risk map draws attention to reaches that have the greatest probability of exceeding the safety threshold. As expected, there is both spatial and temporal variation in the distribution of risk. First, considering the spatial distribution of risk in 2005, there is an

Table 3
Estimated correlation between parameters.

Covariates	Estimated Correlation
L_0, V	0
L_0, S	0
L_0, t	0
V, S	1
t, S	0
V, t	1
L_{ui}, L_{uj}	0.17
ϵ_i, ϵ_j	0.17
L, R	0.35

attenuation of risk as water flows from the outer reaches to the outlet. Depending on the use of the waterways, a water resources manager may decide to change nothing if the outlet meets an acceptable risk level, or implement BMPs only to the high-risk areas. For example, high-risk areas where human contact is more likely to occur might be targeted first.

Note also a difference in risk distribution between the east (park area) and the west (residential). Flows from the western area that have a higher risk of exceedance mix with flows from the eastern area, which can be seen to have a diluting effect, as the outlet risk is lower than in the western areas. Across the years, the park generally has a lower risk, while the residential areas are at higher risk. There is uniformly lower risk in 2006–2008, and uniformly higher risk in 2009 and 2010. From 2005 to 2008, the outlet remains at low risk, while in 2009–2010 the outlet has a moderate risk of exceedance, however the attenuation is still visible.

Risk maps are a useful geospatial tool for water resources managers that provide the spatial context for implementing BMPs for nitrogen management in the watershed. It can help inform decisions about the acceptable risk, as well as the location of higher risk areas. Information about land use in areas with the highest risk helps determine the range of feasible management strategies such as buffer strips and other water runoff reduction measures in both suburban and agricultural areas. The relative importance of locations in terms of use and potential human exposure can be weighed in the decision-making process.

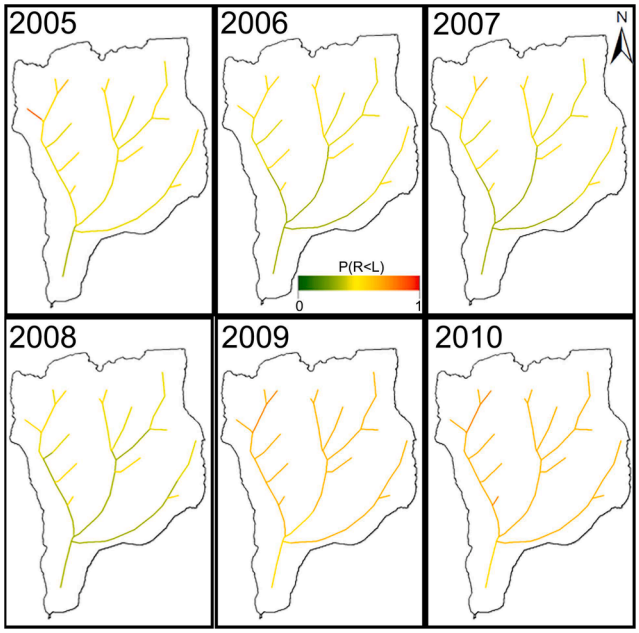

Fig. 5. STREAMS model output - risk maps for TIN in the Shepherd Creek watershed, showing the probability of exceeding a target standard in individual streams represented by the schematic network. Red reaches have a high risk of exceeding the criterion, yellow moderate risk, and green low risk of exceedance. (For interpretation of the references to colour in this figure legend, the reader is referred to the web version of this article.)

The temporal variation in risk distribution can be seen in maps representing different years. One of the two primary factors in risk assessment is the capacity, which is driven by the flow. The cumulative discharge at the outlet along with the average risk across the watershed and at the outlet for 2005–2010 is displayed in Table 4:

In Table 4, there is strong correlation ($\rho = 0.995$, $p < .001$) between the average risk across the watershed and risk at the outlet, however, there is non-significant negative correlation between the discharge and the risk (average risk and discharge $\rho =$ -0.52; $p > .05$, outlet risk and discharge $\rho =$ -0.51; $p > .05$). The attenuation of risk which is visualized in Fig. 5 can also be observed here as the risk at the outlet is consistently lower than the average risk in the watershed. The wide range of flows partially explains the yearly variation in risk. First, the years with lowest discharges (2005, 2009, and 2010) have the highest risks. The lower discharge lowers the capacity which will increase risk without a commensurate reduction in contaminant loading. In 2005, which has the lowest discharge of the studied years, the loading was reduced likely by a decrease in runoff events so the overall risk was not as high as 2009 or 2010. Years 2006–2008 have the lowest average risk, while having increasing discharge. Each subsequent year (2006–2008) has a higher discharge with 2008 having the highest discharge of studied years while having the lowest risk. As discharge increases, capacity increases, which leads to a lowering of risk when the contaminant loading does not commensurately increase. Also, beyond certain discharges the contaminant runoff decreases (Te Chow et al., 2010), and concentration tends to be negatively correlated with the flow (Arheimer et al., 1996; Arheimer and Liden, 2000). Focusing mitigation on initial runoff and washout events may then have a significant impact on the watershed.

3.3.2. *Risk reduction maps*

The effects of different BMP scenarios to decrease risk can also be investigated using STREAMS. For instance, BMP implementation may be effective in decreasing nitrogen loading (Alvarez et al., 2016). BMPs for an area such as Shepherd Creek include buffer strips, rain gardens, proper use of fertilizer, and runoff reduction measures (see for example (Roy et al. (2006); Roy and Shuster (2009))). BMPs can be implemented at specific locations, and resulting changes in risk can be quantified. The effects of some BMPs on nutrient export from land are known (Cho et al., 2010a, 2010b). Then, using the estimated reduction, the respective changes in risk can be quantified. Here, a 15% reduction in TIN runoff from all areas is investigated.

To simulate the application of BMPs, Eq. (2) is modified as:

$$L_{NPS} = \sum_i B_i \epsilon_i A_i \tag{23}$$

where B_i is the percent exported after BMP implementation. This allows STREAMS to apply the BMPs in whatever configuration the user specifies. In this use case, we used $B_i = 0.85$ for a reduction of 15%, which illustrates the maximum attainable effect of BMP implementation in the watershed if a 15% load reduction is achieved across all land uses. Both the mean values and the variability will be affected by the change, which in turn will affect the risk.

The resulting risk reduction maps draw attention to areas that have the greatest potential reduction in risk from a given BMP. The year 2005 shows the highest potential risk reduction; across all years the greater potential for risk reduction falls in the outer reaches in both the residential and park areas. As 2005 had the lowest capacity initially, it makes sense that a change in the watershed would have the largest effect on risk outcomes. The reduction is also greatest in areas that initially had a higher risk, which is of special interest for making decisions about BMPs. By implementing possible BMPs in the areas with high risk and

Table 4
Yearly discharge at the outlet of Shepherd Creek.

Year	Cumulative Discharge at Outlet (10^4 ft^3)	Average Risk across Watershed	Risk at Watershed Outlet
2005	13	0.51	0.35
2006	52	0.49	0.33
2007	65	0.49	0.33
2008	84	0.46	0.32
2009	36	0.66	0.54
2010	42	0.67	0.56

high potential for risk reduction, the impacts on the watershed are maximized. BMP implementation is also subject to feasibility. For example, if runoff areas were accessible for mitigation in the residential area, but not in the park, an optional scenario would be to only place BMPs in the residential area. Further, placing a monitoring station at these locations could be considered to monitor progress.

The years 2009–2010 showed little potential for risk reduction. As discussed earlier, these years have a higher load without proportionately higher capacity. This is the reason behind greater reductions in the higher flow years as seen in 2006–2008 where the load is reduced while the capacity remains high. To reduce risk, especially in years such as 2009–2010, the factors that contribute to it must be addressed. Considering Eqs. (18) and (21), these factors are the mean load and capacity, the variability in the load and the capacity, and the covariance between the capacity and load. Potential ways to reduce loading are discussed above, so here we examine potential reduction in variances. While the variability in the load and capacity are the hardest to influence directly, they scale approximately proportionately with the square of the mean (Haldar and Mahadevan, 2000). This may point to flow reduction measures as a potentially beneficial measure for risk reduction, as higher flows are associated with higher variability and higher loads. Detention and retention ponds, rain gardens, water barrels, reduction in impervious surfaces, and planting of trees may reduce the variability of the flows and loads on small scales which will lead to reduced risk.

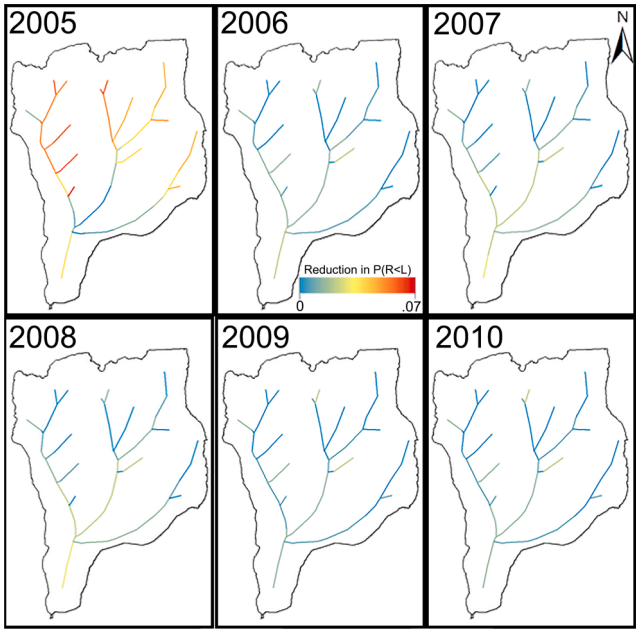

Fig. 6. STREAMS model output - risk reduction maps showing the expected difference in probability of nitrogen load exceedance due to BMP implementation in the entire Shepherd Creek watershed. Red branches show the greatest reduction in risk, yellow - moderate reduction, and blue - low reduction in risk. This information can be used to select the areas where BMPs are likely to make the greatest impact.

The information gained from analyzing the model results illustrates the maximum attainable effect of BMP implementation, with potential importance for the regional economy (Asci et al., 2012; Cools et al., 2011; Xu et al., 2020; Zimmerman et al., 2019). STREAMS can compute changes from this implementation in a single catchment; however, to see the cumulative effects of BMP implementation, watershed-wide evaluation is necessary. STREAMS enables visualization of the difference in nitrogen loads brought about by implementing BMPs, as shown in Fig. 6. This information can be used to target specific areas in the watershed for focused BMP implementation and can contribute to planning for reducing nitrogen loading at the watershed scale.

4. Case study 2 – Upper East Fork watershed

4.1. Study area

The Upper East Fork Watershed (UEFW) is a mixed-use watershed in southwest Ohio. It measures approximately 775 km^2 and drains into a reservoir built in the 1970 s for flood control. The reservoir also serves as a source of drinking water and is a regional recreational resource. Water quality was monitored at 6 sites in 2009 and at 4 additional sites in 2010 on a weekly basis for parameters including nitrogen species, phosphorus, and organic carbon. A flow monitoring station is located on the main stem at ELI leading up to the lake (Fig. 7). This monitoring station has been operational from 2014-present, and for 1980–2013 the estimated flow is available from the USACE-Louisville District's website (https://www.lrl-wc.usace.army.mil/reports/yearly/W.%20H.%20Harsha%20Lake_2009.html).

A large portion of the watershed is used for agriculture that contributes to non-point source nitrogen loading. Additionally, there are 8 major point sources for nitrogen including wastewater treatment plants (WWTPs), which report their contribution to nitrogen loading under National Pollutant Discharge Elimination System (NPDES) permits (data obtained from https://echo.epa.gov/). The reported discharge and ammonia loading is shown in Table 5. Only one WWTPS (site code 1 PB0034) has nitrate-nitrite at the effluent recorded (average of 5.4 mg/

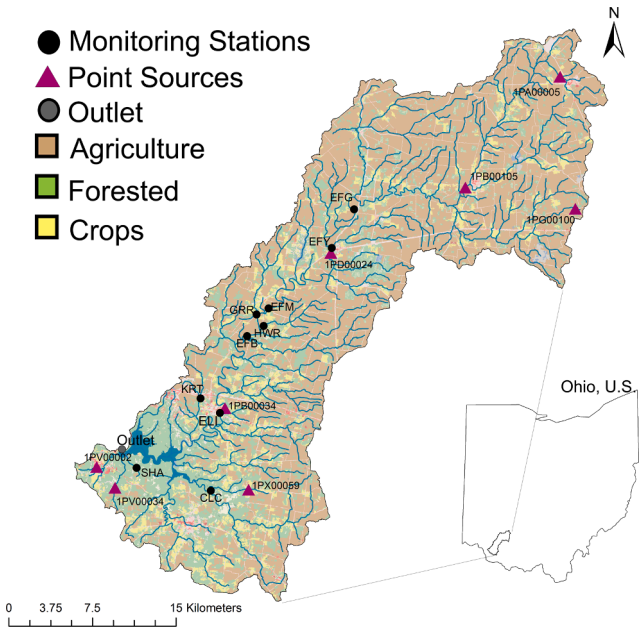

Fig. 7. Upper East Fork Watershed with land uses, monitoring stations, reservoir outlet, and point sources.

Table 5
Point source loading data. Data obtained from echo.epa.gov.

Site Code	Site Name	Facility Actual Average Flow (MGD)		Reported Ammonia Discharge (Kg/year)	
		2009	2010	2009	2010
1PA00005	New Vienna WWTP	0.2732	0.3607	2882	3108
1 PB00034	Williamsburg WWTP	0.2703	0.2484	220	528
1 PB00105	Lynchburg WWTP	0.2019	0.1678	51	118
1PD00024	Fayetteville Perry Twp WWTP	0.1774	0.1185	277	224
1PG00100	Rolling Acres Municipal WWTP	0.0094	0.0104	0	5
1PV00002	Holly Towne MHP	0.0398	0.0352	3	11
1PV00034	Forest Creek MHP	0.0187	0.0163	28	1
1PX00059	Locust Ridge Sewage System	0.0047	0.0038	16	13

l), so in this paper we use 20 mg/L as an estimate of nitrate for the other stations based on Tchobanoglous et al. (2004). Water quality monitoring data used in this example can be accessed using the WaterOneFlow web services developed by CUAHSI HIS in the same manner as the Shepherd Creek data. The years 2009 and 2010 were selected based on availability of monitored water quality data.

4.2. Model parameters and calibration

The difference between modeled and observed concentrations was minimized during calibration. Here, flow data were not available at most of the observation stations, and concentrations were estimated by dividing modeled loads by modeled flows. The minimization was done using the optimization functionality within Excel, using the export coefficients and the spiraling lengths at various flow rates as optimization parameters. The fit of the calibrated concentrations was satisfactory (Fig. 8).

This calibration and validation procedure for the UEFW produced values for both export coefficients from the various land uses and spiraling lengths for different flows. The export coefficients presented in Table 6 are used in conjunction with Eq. (11). These values fall within published ranges of nitrogen export coefficients (Lin, 2004; Saad et al., 2011; Schwarz et al., 2009), and are further used in Eq. (11) to calculate mean loading.

Calibrated spiraling length values for Eq. (10) are presented in Table 7, and are also consistent with reported values (Ensign and Doyle, 2006; Runkel, 2007).

The estimated coefficients of variation and the covariances are the same as Tables 2a, 2b, and 3 from Shepherd Creek. The covariances needed for $Var(L_{PS})$ were calculated directly from the data available from WWTPs using Eq. (14). As with the previous case study, we verify the accuracy of the first order approximation by comparing its output to the output of the Monte Carlo simulation using the same input parameters as the first-order approximation. This produces a NSE of 0.52 across all links. The ELI station flow data was used for determining the weighting factors: 2009 was 1.03 times the average, and 2010 was 0.86 times the average. The estimated flows at ELI had a RMSE of 3.53 cfs.

4.3. Results and discussion

4.3.1. Risk maps

Fig. 9 shows the STREAMS output as a risk map for the UEFW produced for 2009.

The STREAMS risk map of the UEFW shows many of the headwater areas having higher risk; however the forested area near the reservoir is generally at lower risk. The lower risk is due to the lower amount of loading in those areas as the forested areas have the lowest export coefficient while the agricultural areas have the highest. There are areas of the main stem that have a higher risk, but it attenuates before reaching the reservoir. Natural uptake and dilution can both lead to risk decrease. A watershed manager would need to decide if and where having a higher risk is acceptable. If maintaining high quality of water in the reservoir is the main objective, then higher risk in the upper areas of the main stem could be acceptable. However, if a uniform risk criterion is applied

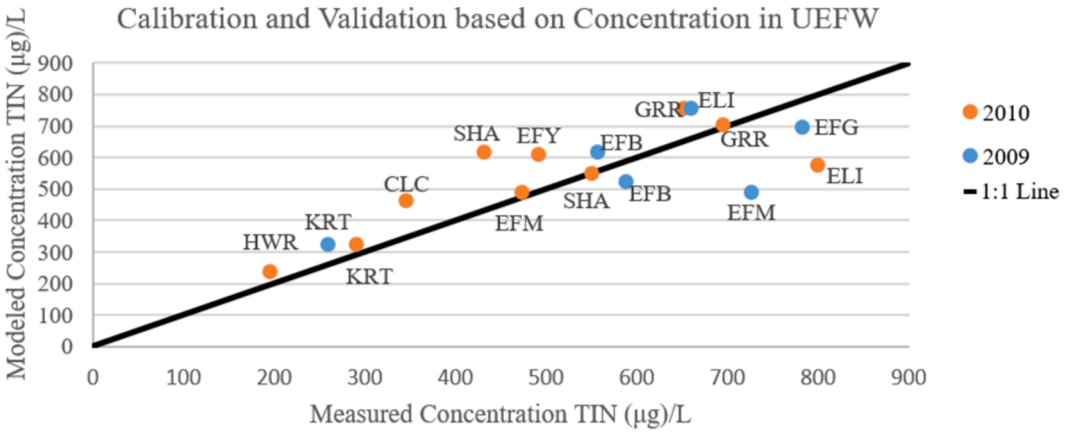

Year	NSE for Concentration
2009 (calibration year)	0.60
2010 (validation year)	0.50

Fig. 8. Calibration and validation performance for the UEFW. Calibration was performed on 2009 for the concentration data.

Table 6
Export coefficients of nitrogen used for various land use types.

Land Use (Based on NLCD2006)	Mean Export Coefficient μ_{e_i} (kg of TIN/ha/year)	
	Reported Range in Literature	Used in this Study
Forested	1 – 15	2.1
Row Crops	2 – 80	8.4
Mixed Agriculture	2 – 80	8.2
Urban	2 – 41	5.4
Residential	0.1 – 14	5.1
Commercial	0.1 – 14	5.4
Industrial	0.1 – 14	2.3
Barren	0.5 – 20	4.9

Table 7
Spiraling lengths at different flow rates used in this study.

Flow (cfs)	Mean Spiraling Length (m)
1–50	200
50–100	150
100–300	200
300+	800

across the watershed, then the higher risk areas will need to be addressed. There are also differences across years to consider, as 2010 has higher risk, especially in the agricultural areas. The lower streamflow for 2010 seems to be the main factor that leads to these higher risks.

Many of the first-order reaches in the agricultural areas have high probabilities of exceeding the target. These are the areas where the contaminant load initially gets delivered into the network, with no opportunity for dilution or removal. These areas have some of the highest loads relative to the capacity, which is due to the high amount exported while having a lower flow. The main stem of the UEFW accumulates loads throughout the watershed such that the highest load in the watershed is at the outlet to the reservoir. The main stem segment leading up to the reservoir has a lower risk of exceedance even though it has the highest load. This is due to the capacity being higher than the loading. As water travels through the reaches, uptake and dilution occur, which lowers the probability of exceedance.

So, although the highest amount of nitrogen is delivered through the main stem into the reservoir, the highest risk occurs elsewhere, as the risk map illustrates. Here, risk maps highlight areas that not just have the highest load, but also the highest probability of exceeding the safety threshold.

Another area of interest includes the regions of the main stem that change from high risk into low risk (*i.e.* upstream of the main stem of station EFG, as well as between EFB and ELI). These dynamics would not be seen in model results that only show load. The watershed manager can decide from these findings if having high-risk reaches is acceptable, or that the naturally occurring attenuation is sufficient for downstream purposes.

4.3.2. Risk reduction maps

The methodology demonstrated with the Shepherd Creek watershed is applied here as well. Possible BMPs that could be used in this area include buffer strips, optimal fertilizer practices, and ensuring manure and waste system detention. A 15% reduction is applied only to agricultural areas, and the prospective effects of BMP practices and the results are displayed in Fig. 10.

The implementation of BMPs has a visibly large impact primarily on the upper parts of the main stem, as the dark red regions show a 35% reduction in risk in both 2009 and 2010. Some of the first-order streams in the agricultural area only show a 15%-20% risk reduction from BMP implementation. This is likely because there is not as much opportunity for cumulative reduction due to benefits from upstream BMPs, unlike the changes seen in the upper third of the main stem. In addition to the reduction in load from BMPs, further reduction occurs through uptake. Additionally, loads from high-risk streams mixing with those from lower risk streams reduce the overall risk. All of these factors collectively contribute to the reduction of risk in the main stem. There are also some differences across years. Years 2009 and 2010 have in common the locations where the reduction in risk primarily happens. However, in 2010 risk is not reduced as much as in 2009, even though 2010 has higher initial risk. This is likely due to the additional capacity generated by higher flows in 2009 as compared to 2010.

Watershed managers can use information that STREAMS produces to help inform planning decisions. Having the high-risk areas be the most attenuated by BMPs provides a potential scenario for the managers to consider. They may find it acceptable to only implement changes in the upper third of the watershed as this would produce results for that area and also reduce risk downstream. This alternative scenario to BMP implementation throughout the entire watershed could also be simply simulated using STREAMS. The placement of additional monitoring stations for this area, as well as continued use of current stations, could be considered to monitor progress. The final decisions should be made

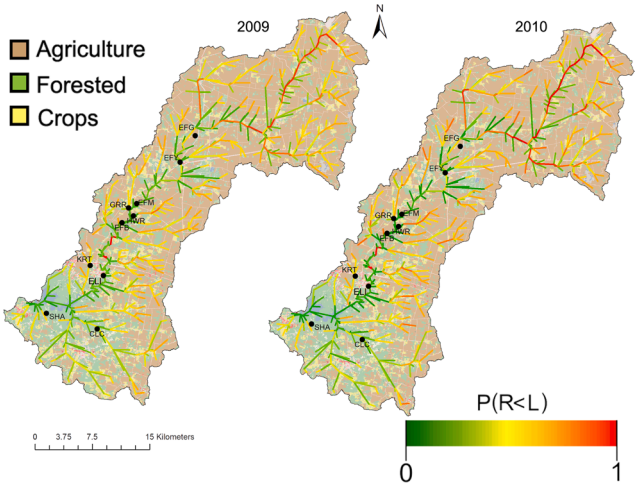

Fig. 9. STREAMS risk map of the Upper East Fork Watershed for 2009 and 2010. Dark red indicates a high risk of exceeding the safety threshold, while green indicates low risk.

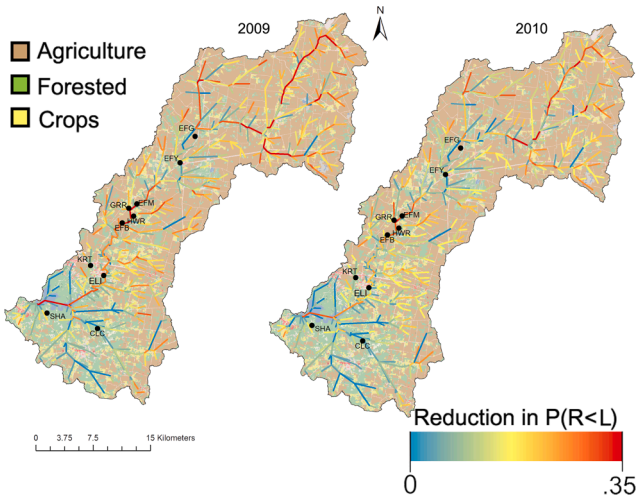

Fig. 10. STREAMS model output - risk reduction map of the Upper East Fork Watershed for 2009 and 2010. The darker red areas show a higher reduction in risk, the yellow a moderate change in risk, and the blue a low change in risk.

based on STREAMS results augmented by the cost-benefit analysis of different management options.

5. Conclusions

This paper presents STREAMS (STochastic Reliability-based Risk Evaluation And Mapping for watershed Systems and Sustainability), a spatially distributed, reliability-based approach to compute and visualize water contamination risk at a watershed scale. Inspired by spatial visualization of the chance of rain in weather maps, STREAMS output is mapped to visualize risk of water contamination in watersheds. STREAMS expands the computational capabilities of ArcGIS geospatial processing tools, which serve as a platform to integrate a watershed-scale nitrogen transport model with reliability-based risk assessment. As a result, STREAMS is an intuitive and visually compelling decision-making tool. It is expected to facilitate communication of risk to stakeholders and provide insights into the spatial distribution of risk, as well as changes in risk as best management practices are simulated and tested. The results enable identification of vulnerable, high-risk sites within the watershed where water quality remediation could be implemented. It allows watershed managers to make decisions based on the reduction in risk and location of that reduction, which in turn enables targeting and protecting these areas effectively and efficiently. The general public can also view and understand these maps in deciding recreational safety and raising awareness. STREAMS can be extended to a wide range of contaminants, and can also be linked to real-time models so that timely advisories can be implemented for acute contamination events.

Declaration of Competing Interest

The authors declare that they have no known competing financial interests or personal relationships that could have appeared to influence the work reported in this paper.

Acknowledgement and disclaimer

The authors gratefully acknowledge funding from National Science Foundation (CBET-1351361). We also thank William Shuster for the Shepherd Creek dataset as well as insightful discussions. The U.S. Environmental Protection Agency (USEPA), through its Office of Research and Development, partially funded and collaborated in the research described herein. Any opinions expressed in this paper are those of the author(s) and do not reflect the views of the Agency, therefore, no official endorsement should be inferred. Any mention of trade names or commercial products does not constitute endorsement or recommendation for use by the USEPA.

Appendix:. Nomenclature

Parameter	Definition
L_{total}	Total input load at the given catchment
L_{NPS}	Non-point sources load
L_{PS}	Point sources load
L_u	Upstream load
$\in_i$	Export coefficient
A_i	Area
m	Number of land uses in a catchment
C_y	Concentration at distancey
C_0	Initial Concentration
Q_y	Flow at distancey
Q_0	Initial Flow

(*continued on next page*)

(*continued*)

Parameter	Definition
s	Spiraling length
Y	Distance
Q	Flow
λ	Decay rate
V	Flow velocity
t	Time (to travel distance y at velocity V)
$\mathbb{r}$	Reach
$L_{\mathbb{r}}$	Contaminant load at end of reach$\mathbb{r}$
L_0	Initial load
L	Load
Z	A stochastic variable
$X_1, X_2, \cdots, X_n$	Stochastic variables
$g()$	A function of variables
$\mu_{X_1}, \mu_{X_2}, \cdots, \mu_{X_n}$	Mean of X_i, $i = 1,\ldots,n$
μ_{X_j}	Mean of X_j
$\mu_{L_{\mathbb{r}}}$	Mean of L at end of reach$\mathbb{r}$
μ_{L_0}	Mean ofL_0
μ_V	Mean of$V$
μ_S	Mean of$S$
μ_t	Mean of$t$
μ_{ϵ_i}	Mean ofϵ_i
$\mu_{L_{PS\,\imath}}$	the $\imath$th mean point-source input
$\aleph$	Number of point sources at some node
$\imath$	Index used with point sources
$\mu_{L_{u\,\prime}}$	mean upstream load for the $\prime$th upstream branch
$\prime$	Index used for upstream branches
η	Number of upstream input branches at some node
$\mathbb{Z}$	Set of all integers
Q_{PS}	Measured flow
C_{PS}	Measured Concentration
$\mu_{C_{PS}}$	Mean of the measured concentration from a point source
$\mu_{Q_{PS}}$	Mean of the measured flow from a point source
CV	Coefficient of variation
$CV_{L_{\mathbb{r}}}$	Coefficient of variation of the load in stream link$\mathbb{r}$
$p_{f_{\mathbb{r}}}$	Probability of failure for link (reach)$\mathbb{r}$
$R_{\mathbb{r}}$	capacity or resistance in reach$\mathbb{r}$
$L_{\mathbb{r}}$	Contaminant load in reach$\mathbb{r}$
R	Capacity, a random variable
L	Load, a random variable
p_f	Probability of failure
L'	Load transformed into standard normal variate
R'	Capacity transformed into standard normal variate
y*	The most probable point of failure in FORM algorithm
B	The minimum distance between the origin and the performance function in FORM algorithm
C_T	Safety concentration threshold
$\mu_{R_{\mathbb{r}}}$	Mean of capacity of reach$\mathbb{r}$
$\mu_{Q_{\mathbb{r}}}$	Mean flow in reach$\mathbb{r}$
$\mu_{L_{\mathbb{r}}}$	Mean of load in reach$\mathbb{r}$
$CV_{R_{\mathbb{r}}}$	Coefficient of variation of capacity in reach$\mathbb{r}$
$CV_{L_{\mathbb{r}}}$	Coefficient of variation of load in reach$\mathbb{r}$
CV_R	Coefficient of variation of capacity
CV_L	Coefficient of variation of load
$\Phi()$	Cumulative distribution function of the standard normal variate
ρ	Correlation coefficient
B_i	BMP export percent

Appendix A. Supplementary data

Supplementary data to this article can be found online at https://doi.org/10.1016/j.jhydrol.2021.126030.

References

Abrishamchi, A., Tajrishy, M., Shafieian, P., 2005. Uncertainty Analysis in QUAL2E Model of Zayandeh-Rood River. Water Environ. Res. 77 (3), 279–286.

Ahmadisharaf, E., Benham, B.L., 2020. Risk-based decision making to evaluate pollutant reduction scenarios. Sci. Total Environ. 702, 135022.

Ahmadisharaf, E., Camacho, R.A., Zhang, H.X., Hantush, M.M., Mohamoud, Y.M., 2019. Calibration and validation of watershed models and advances in uncertainty analysis in TMDL studies. J. Hydrol. Eng. 24 (7), 03119001.

Ahn, K.-H., Merwade, V., 2014. Quantifying the relative impact of climate and human activities on streamflow. J. Hydrol. 515, 257–266.

Alarcon, V.J., McAnally, W., Ervin, G., Brooks, C., 2010. Using MODIS land-use/land-cover data and hydrological modeling for estimating nutrient concentrations. In: International Conference on Computational Science and Its Applications. Springer, pp. 501–514.

Alvarez, S., Asci, S., Vorotnikova, E., 2016. Valuing the potential benefits of water quality improvements in watersheds affected by non-point source pollution. Water 8 (4), 112.

Ames, D.P., et al., 2012. HydroDesktop: Web services-based software for hydrologic data discovery, download, visualization, and analysis. Environ. Modell. Software 37, 146–156.
Arheimer, B., Andersson, L., Lepistö, A., 1996. Variation of nitrogen concentration in forest streams—influences of flow, seasonality and catchment characteristics. J. Hydrol. 179 (1–4), 281–304.
Arheimer, B., Liden, R., 2000. Nitrogen and phosphorus concentrations from agricultural catchments—influence of spatial and temporal variables. J. Hydrol. 227 (1–4), 140–159.
Asci, S., Borisova, T., VanSickle, J.J., Zotarelli, L., 2012. Risk and nitrogen application decisions in Florida potato production.
Beaulac, M.N., Reckhow, K.H., 1982. An examination of land use-nutrient export relationships 1. JAWRA J. Am. Water Resour. Assoc. 18 (6), 1013–1024.
Beck, M.B., 2013. Water quality management: A review of the development and application of mathematical models, 11. Springer Science & Business Media.
Besaw, L.E., Rizzo, D.M., Bierman, P.R., Hackett, W.R., 2010. Advances in ungauged streamflow prediction using artificial neural networks. J. Hydrol. 386 (1–4), 27–37.
Bicknell, B.R., Imhoff, J.C., Kittle, J.L., Donigian, A.S., Johanson, R.C., 1997. Hydrological Simulation Program-Fortran, User's manual for version 11. National Exposure Research Laboratory, Athens, Ga.
Borsuk, M.E., Stow, C.A., Reckhow, K.H., 2002. Predicting the frequency of water quality standard violations: a probabilistic approach for TMDL development. Environ. Sci. Technol. 36 (10), 2109–2115.
Bourinet, J., Mattrand, C., Dubourg, V., 2009. A review of recent features and improvements added to FERUM software. Proc of the 10th International Conference on Structural Safety and Reliability (ICOSSAR'09).
Brosch, C., 2010. Estimates of County-Level Nitrogen and Phosphorus Data for use in Modeling Pollutant Reduction Documentation for Scenario Builder Version 2.2.
Camacho, R.A., Martin, J.L., Wool, T., Singh, V.P., 2018. A framework for uncertainty and risk analysis in total maximum daily load applications. Environ. Modell. Software 101, 218–235.
Chambers, P.A., et al., 2012. Development of environmental thresholds for nitrogen and phosphorus in streams. J. Environ. Qual. 41 (1), 7–20.
Chin, D., 2009. Rink-Based TMDLs in Pathogen-Impaired Waters. J. Water Resour. Plann. Manage. 521–527.
Cho, J., et al., 2010a. Effect of watershed subdivision and filter width on swat simulation of a coastal plain watershed. JAWRA 46 (3), 586–602. https://doi.org/10.1111/j.1752-1688.2010.00436.x.
Cho, J., Vellidis, G., Bosch, D.D., Lowrance, R.R., Strickland, T.C., 2010b. Water quality effects of simulated conservation practice scenarios in the Little River Experimental watershed. J. Soil Water Conserv. 65 (6), 463–473. https://doi.org/10.2489/jswc.65.6.463.
Cools, J., et al., 2011. Coupling a hydrological water quality model and an economic optimization model to set up a cost-effective emission reduction scenario for nitrogen. Environ. Modell. Software 26 (1), 44–51.
Cowan, N., et al., 2019. Nitrogen use efficiency and N2O and NH3 losses attributed to three fertiliser types applied to an intensively managed silage crop. Biogeosciences 16 (23), 4731–4745.
Daniel, E.B., et al., 2011. Watershed modeling and its applications: a state-of-the-art review. Open Hydrol. J. 5 (1).
Dey, P., Mishra, A., 2017. Separating the impacts of climate change and human activities on streamflow: a review of methodologies and critical assumptions. J. Hydrol. 548, 278–290.
Dilks, D.W., Feedman, P.L., 2004. Improved consideration of the margin of safety in total maximum daily load development. J. Environ. Eng. 130 (6), 690–694.
Ensign, S.H., Doyle, M.W., 2006. Nutrient spiraling in streams and river networks. J. Geophys. Res. 111 (G4), 1–13. https://doi.org/10.1029/2005JG000114.
EPA, 1999. Protocol for Developing Nutrient TMDLs. Office of Water, Washington DC.
Evans-White, M., Haggard, B., Scott, J., 2013. A review of stream nutrient criteria development in the United States. J. Environ. Qual. 42 (4), 1002–1014.
Franceschini, S., Tsai, C., 2008. Incorporating reliability into the definition of the MOS in TMDL calculations. J. Water Resour. Plann. Manage. 34–44.
Francesconi, W., Srinivasan, R., Pérez-Miñana, E., Willcock, S.P., Quintero, M., 2016. Using the Soil and Water Assessment Tool (SWAT) to model ecosystem services: a systematic review. J. Hydrol. 535, 625–636.
Gandolfi, C., Facchi, A., Whelan, M.J., 2001. On the relative role of hydrodynamic dispersion for river water quality. Water Resour. Res. 37 (9), 2365–2375. https://doi.org/10.1029/2001WR000249.
Gerland, P., et al., 2014. World population stabilization unlikely this century. Science 346 (6206), 234–237.
Goudie, A.S., 2018. Human impact on the natural environment. John Wiley & Sons.
Haldar, A., Mahadevan, S., 2000. Probability, Reliability and Statistical Methods in Engineering Design. John Wiley & Sons, New York, 304 pp.
Hall, R.O., et al., 2009. Nitrate removal in stream ecosystems measured by 15N addition experiments: Total uptake. Limnol. Oceanogr. 54 (3), 653–665.
Hamed, M.M., El-Beshry, M.Z., 2004. Uncertainty analysis in dissolved oxygen modeling in streams. Environ. Manage. 34 (2), 233–244.
Hoque, Y.M., Tripathi, S., Hantush, M.M., Govindaraju, R.S., 2012. Watershed reliability, resilience and vulnerability analysis under uncertainty using water quality data. J. Environ. Manage. 109, 101–112.
Huo, S., et al., 2018. Development of methods for establishing nutrient criteria in lakes and reservoirs: a review. J. Environ. Sci. 67, 54–66.
Jakeman, A., Littlewood, I., Whitehead, P., 1990. Computation of the instantaneous unit hydrograph and identifiable component flows with application to two small upland catchments. J. Hydrol. 117 (1–4), 275–300.
Jobson, H.E., 1996. Prediction of Traveltime and Longitudinal Dispersion in Rivers and Streams.
Johnson, S.L., Maidment, D.R., Kirisits, M.J., 2013. TMDL balance: a model for coastal water pollutant loadings. JAWRA J. Am. Water Resour. Assoc.
Koltun, G.F., Whitehead, M.T., 2002. Techniques for Estimating Selected Streamflow Characteristics of Rural, Unregulated Streams in Ohio. FHWA/OH-2001/13, USGS.
Kriegesmann, B., 2012. Probabilistic design of thin-walled fiber composite structures, Technische Informationsbibliothek und Universitätsbibliothek Hannover (TIB).
Langseth, D.E., Brown, N., 2010. Risk-Based Margins of Safety for Phosphorus TMDLs in Lakes. J. Water Resour. Plann. Manage. 137 (3), 276–283.
Levy, P., et al., 2017. Estimation of cumulative fluxes of nitrous oxide: uncertainty in temporal upscaling and emission factors. Eur. J. Soil Sci. 68 (4), 400–411.
Limpert, E., Stahel, W.A., Abbt, M., 2001. Log-normal distributions across the sciences: keys and clues. Bioscience 51 (5), 341–352.
Lin, J., 2004. Review of Puclished Export Coeficient and Event Mean Concentration (EMC) Data, Wetlands Regulatory Assistance. Program.
Loehr, R., 1989. Estimating the nutrient load to a water body. The control of eutrophication of lakes and reservoirs 115–146.
Maier, H.R., Lence, B.J., Tolson, B.A., Foschi, R.O., 2001. First-order reliability method for estimating reliability, vulnerability, and resilience. Water Resour. Res. 37 (3), 779–790.
Martin, G.R., Arihood, L.D., 2010. Methods for estimating selected low-flow frequency statistics for unregulated streams in Kentucky. U. S, Geological Survey.
Maskey, S., Guinot, V., 2003. Improved first-order second moment method for uncertainty estimation in flood forecasting. Hydrol. Sci. J. 48 (2), 183–196.
McKay, L., et al., 2012. NHDPlus version 2: User guide. US Environmental Protection Agency.
Messinger, T., Paybins, K.S., 2014. Correlations of daily flows at streamgages in and near West Virginia, 1930-2011, and streamflow characteristics relevant to the use of index streamgages. US Geological Survey.
Miltner, R., 2010. A method and rationale for deriving nutrient criteria for small rivers and streams in Ohio. Environ. Manage. 45 (4), 842–855.
Mishra, A., et al., 2019. Two-phase Monte Carlo simulation for partitioning the effects of epistemic and aleatory uncertainty in TMDL modeling. J. Hydrol. Eng. 24 (1), 04018058.
Moriasi, D.N., et al., 2007. Model Evaluation Guideines for Systematic Quantification of Accuracy in Watershed Simulations. Trans. ASABE 50 (3), 885–900.
Nash, J.E., Sutcliffe, J.V., 1970. River flow forecasting through conceptual models part I — A discussion of principles. J. Hydrol. 10 (3), 282–290.
Neitsch, S.L., Arnold, J.G., Kiniry, J.R., Williams, J.R., 2011. Soil and Water Assessment Tool Theoretical Documentation. Texas A&M, Texas.
Nelson, E., et al., 2009. Modeling multiple ecosystem services, biodiversity conservation, commodity production, and tradeoffs at landscape scales. Front. Ecol. Environ. 7 (1), 4–11.
Ng, T.L., Eheart, J.W., 2005. Effects of discharge permit trading on water quality reliability. J. Water Resour. Plann. Manage. 131 (2), 81–88.
Park, Y., Yeghiazarian, L., Stedinger, J.R., Montemagno, C.D., 2008. Numerical approach to Cryptosporidium risk assessment using reliability method. Stoch. Env. Res. Risk Assess. 22 (2), 169–183.
Raftery, A.E., Alkema, L., Gerland, P., 2014. Bayesian population projections for the United Nations. Statistical science: a review journal of the Institute of Mathematical Statistics 29 (1), 58.
Reckhow, K.H., Beaulac, M.N., Simpson, J.T., 1980. Modeling phosphorus loading and lake response under uncertainty: A manual and compilation of export coefficients. U. S, EPA, Office of Water Regulations.
Riasi, M.S., Teklitz, A., Shuster, W., Nietch, C., Yeghiazarian, L., 2018. Reliability-based water quality assessment with load resistance factor design: application to TMDL. J. Hydrol. Eng. 23 (12), 04018053.
Robertson, D.M., Saad, D.A., 2011. Nutrient inputs to the laurentian great lakes by source and watershed estimated using SPARROW watershed models. JAWRA J Am Water Resour Assoc 47 (5), 1011–1033.
Roy, A.H., et al., 2006. Retrofit stormwater management: navigating multidisciplinary hurdles at the watershed scale. Stormwater 7, 16–29.
Roy, A.H., Shuster, W.D., 2009. Assessing impervious surface connectivity and applications for watershed management. JAWRA J Am Water Resour Assoc 45 (1), 198–209.
Runkel, R., 2007. Toward a transport-based analysis of nutrient spiraling and uptake in streams. Limnol. Oceanogr. Methods, 50–62.
Saad, D.A., Schwarz, G.E., Robertson, D.M., Booth, N.L., 2011. A Multi-Agency Nutrient Dataset Used To Estimate Loads, Improve Monitoring Design, And Calibrate Regional Nutrient Sparrow Models. Journal of the American Water Resources Association, 47 (5): 933-949. DOI:0.1111/j.1752-1688. 2011.00575.x.
Safwat, A.M., 2014. Stochastic multimedia modelling of watershed-scale microbial transport in surface water. University of Cincinnati.
Schwarz, G.E., Hoos, A.B., Alexander, R.B., Smith, R.A., 2009. The SPARROW Surface Water-Quality Model: Theory, Application and User Documentation. U.S Geological Survey, Reston, Virginia.
Shanhu, J., et al., 2011. Quantifying the effects of climate variability and human activities on runoff from the Laohahe basin in northern China using three different methods. Hydrol. Process. 25 (16), 2492–2505.
Shirmohammadi, A., 2006. Uncertainty in TMDL models. Trans. ASABME 1033–1049.
Shrestha, S., Kazama, F., Newham, L.T., 2008. A framework for estimating pollutant export coefficients from long-term in-stream water quality monitoring data. Environ. Modell. Software 23 (2), 182–194.

Sitar, N., Cawlfield, J.D., Der Kiureghian, A., 1987. First-order reliability approach to stochastic analysis of subsurface flow and contaminant transport. Water Resour. Res. 23 (5), 794–804.
Stream Solute Workshop, 1990. Concepts and methods for assessing solute dynamics in stream ecosystems. J. North Am. Benthol. Soc. 9 (2), 95–119.
Stuckey, M.H., Koerkle, E.H., Ulrich, J., 2012. Estimation of baseline daily mean streamflows for ungaged locations on Pennsylvania streams, water years 1960–2008. US Department of the Interior, US Geological Survey.
Suplee, M.W., Varghese, A., Cleland, J., 2007. Developing Nutrient Criteria For Streams: An Evaluation Of The Frequency Distribution Method. Journal of the American Water Resources Association, 43(2): 453-472. DOI:10.1111 . j.1752-1688.2007.00036.x.
Tarboton, D.G., et al., 2009. Development of a Community Hydrologic Information System, 18th World IMACS/MODSIM Congress. Cairns, Australia.
Tavakoly Zadeh, A.A., 2014. Flow and transport modeling in large river networks.
Taylor, G.D., Fletcher, T.D., Wong, T.H.F., Breen, P.F., Duncan, H.P., 2005. Nitrogen composition in urban runoff—implications for stormwater management. Water Res. 39, 1982–1989. https://doi.org/10.1016/j.watres.2005.03.022.
Tchobanoglous, G., Burton, F.L., Metcalf, E., Stensel, H.D., 2004. Wastewater Engineering: Treatment and Reuse. McGraw-Hill Education.
Te Chow, V., Maidment, D.R., Mays, L.W., 2010. Applied Hydrology. Tata McGraw-Hill Education.
Teklitz, A., 2016. Reliability approach to risk management in watersheds. University of Cincinnati.
Teklitz, A., Nietch, C., Riasi, M.S., Yeghiazarian, L., 2020. Reliability theory for microbial water quality and sustainability assessment. J. Hydrol.
Thorndahl, S., Schaarup-Jensen, K., Jensen, J.B., 2008. Probabilistic modelling of combined sewer overflow using the First Order Reliability Method. Water Sci. Technol. 57 (9), 1337–1344.
Tsai, C.W., Franceschini, S., 2005. Evaluation of probabilistic point estimate methods in uncertainty analysis for environmental engineering applications. J. Environ. Eng. 131 (3), 387–395.
Tung, Y.K., Mays, L., 1980. Risk analysis for hydraulic design. ASCE J Hydraul Div American Society of Civil Engineers (ASCE) 893–913.
U.S.EPA, 2001. PLOAD user's manual, version 3.
VanSickle, J., Stoddard, J.L., Paulsen, S.G., Olsen, A.R., 2009. Using relative risk to compare the effects of aquatic stressors at a regional scale. Environ. Manage. 38, 1020–1030. https://doi.org/10.1007/s00267-005-0240-0.
Vogel, R.M., Wilson, I., Daly, C., 1999. Regional regression models of annual streamflow for the United States. J. Irrig. Drain. Eng. 125 (3), 148–157.
Wagner, B.J., Gorelick, S.M., 1987. Optimal groundwater quality management under parameter uncertainty. Water Resour. Res. 23 (7), 1162–1174.
Wang, Y.C., Chen, S.T., Yu, P.S., Yang, T.C., 2008. Storm-event rainfall–runoff modelling approach for ungauged sites in Taiwan. Hydrol. Process. 22 (21), 4322–4330.
Whiteaker, T., 2006. Integrating Arc Hydro Features with a Schematic Network. Transaction in GIS 10 (2), 219–237.
Xu, Y., Bosch, D.J., Wagena, M.B., Collick, A., Easton, Z.M., 2020. Reducing nitrogen control costs by within-and cross-county targeting. J. Environ. Manage. 263, 110333.
Yang, G., Best, E.P., Whiteaker, T., Teklitz, A., Yeghiazarian, L., 2014. A screening-level modeling approach to estimate nitrogen loading and standard exceedance risk, with application to the Tippecanoe River watershed, Indiana. J. Environ. Manage. 135, 1–10.
Yeghiazarian, L., 2006. A combined microscopic and macroscopic approach to moseling the transport of pathogenic microorganisms from nonpoint sources of pollution. Water Resour. Research(42).
Yeghiazarian, L. et al., 2013. Environmental data management in support of sharing data and management. , Cincinnati, Ohio.
Yeonjeong, P., Yeghiazarian, L., Stedinger, J., Montemagno, C., 2007. Numerical approach to Cryptosporidium risk assessment using reliability method. Sochastic Environmental Research Risk Assment.
Yongfang, Z., et al., 2011. Analysis of impacts of climate variability and human activity on streamflow for a river basin in northeast China. J. Hydrol. 510 (3), 239–247.
Young, A.R., 2006. Stream flow simulation within UK ungauged catchments using a daily rainfall-runoff model. J. Hydrol. 320 (1–2), 155–172.
Zhang, X., Zhang., M., 2011. Modeling effectiveness of agricultural BMPs to reduce sediment load and organophosphate pesticides in surface runoff. Sci. Total Environ. 409 (10), 1949–1958.
Zimmerman, E.K., Tyndall, J.C., Schulte, L.A., 2019. Using spatially targeted conservation to evaluate nitrogen reduction and economic opportunities for best management practice placement in agricultural landscapes. Environ. Manage. 64 (3), 313–328.